Science in China Series B: Chemistry

www.scichina.com
chem.scichina.com
www.springerlink.com

Photothermal ablation therapy for cancer based on metal nanostructures

ROZANOVA Nadejda† & ZHANG JinZhong†

Department of Chemistry and Biochemistry, University of California, Santa Cruz, CA 95064, USA

Besides conventional surgery, radiation therapy, and chemotherapy, which all tend to have side-effects and damage normal tissues, new medical strategies, such as photothermal sensitization and photothermal ablation therapy (PTA) with near-IR laser light, have been explored for treating cancer. Much of the current excitement surrounding nanoscience is directly connected to the promise of new nanotechnology for cancer diagnosis and therapy. The basic principle behind PTA is that heat generated from light can be used to destroy cancer cells. Strong optical absorption and high efficiency of photothermal conversion at the cancer sites are critical to the success of PTA. Because of their unique optical properties, e.g., strong surface plasmon resonance (SPR) absorption, noble metal nanomaterials, such as gold and silver, have been found to significantly enhance photothermal conversion for PTA applications. Substantial effort has been made to develop metal nanostructures with optimal structural and photothermal properties. Ideal metal nanostructures should have strong and tunable SPR, be easy to deliver, have low toxicity, and be convenient for bioconjugation for actively targeting specific cancer cells. This review would highlight some gold nanostructures with various shapes and properties, including nanoparticles (NPs), nanorods (NRs), nanoshells, nanocages, and hollow nanospheres, which have been studied for PTA applications. Among these structures, hollow gold nanospheres (HGNs) exhibit arguably the best combined properties because of their small size (30—50 nm), spherical shape, and strong, narrow, and tunable SPR absorption.

1 Introduction

Cancer remains one of the most deadly and challenging diseases in the world. Cancer rates could further increase by 50% to 15 million new cases in the next decade, according to the World Cancer Report (3 April 2003, Geneva), the most complete global examination of the disease to date. In the year 2000, malignant tumors were responsible for 12% of the nearly 56 million deaths worldwide from all causes. In many countries, more than a quarter of deaths are attributable to cancer. In 2000, men (5.3 million) and women (4.7 million) developed malignant tumors and 6.2 million died from the disease. To fight the battle of cancer, more and better diagnostic and treatment modalities must be developed.

In the last several decades, significant effort has been made to develop therapeutic methods based on light or laser for detecting and treating cancer. Some of these techniques have the potential for operating at the level of single cells[1−4]. In these methods, only cancer cells are specifically targeted based on their abnormality, while normal cells are unaffected. Photochemical, photomechanical, and photothermal effects of laser interactions with cells and tissues are the basis for many of these techniques[5−9]. For example, photodynamic therapy (PDT) uses photoactivation of specific chemical agents

Received July 12, 2009; accepted September 2, 2009
doi: 10.1007/s11426-009-0247-0
†Corresponding author (email: zhang@chemistry.ucsc.edu)
Supported by the US NSF, US DoD, and NASA UARC

to produce single state oxygen or radicals that are cytotoxic for surrounding cells and tissues, which can be used for cancer treatment[10−12]. Likewise, photomechanical therapy uses laser-induced breakdown for cancer treatment[13,14]. Photothermal ablation (PTA) therapy is another promising technique for cancer therapy that uses heat generated from light to cause damage to cancer cells[15−24].

PTA can operate in three basic modes: i) light only; ii) light with molecules for photothermal conversion; and iii) light with metal nanostructures for photothermal conversion. Generation of shock waves or cavitation-induced heating from photoexcitation has been suggested to be responsible for cell damage[25,26]. Because of the high photothermal conversion efficiency of metal, the third approach is the most effective in terms of heat generation. However, it does involve issues such as delivery to target cancer sites and potential toxicity and side effects of metal nanostructures. Using strategies such as antibody-antigen or ligand-receptor interaction, one can actively target and deliver the metal nanostructures to specific cancer tissues[27,28]. Metals such as gold and silver are considered as biocompatible and low in toxicity and do have good potential for PTA applications.

For instance, it has recently been established that laser-induced local heating of cellular structures through PTA using either pulsed or continuous laser radiation and mediated by light-absorbing nanoparticles (NPs) and microparticles can provide precisely localized damage limited to even single cells[5,29−32]. Accumulation of light-absorbing nanoparticles in relatively transparent cells can enhance their optical absorption up to several orders of magnitude. Thus, metal nanoparticles act as localized sources for photothermal generation that can result in cell damage.

To realize the full therapeutic potential of PTA, the development of novel photothermal coupling agents is essential for increasing its efficiency, decreasing energy dose of laser light, and minimizing potential damage to surrounding normal tissue. Nanostructures of noble metals, such as gold and silver, can exhibit strong optical absorption in the near-IR (NIR, 700−900 nm), when produced in appropriate structures; and the NIR region is desired for minimal absorption or optimal penetration of tissue[15−17,19−22]. It has been demonstrated that the efficiency of PTA can be enhanced when the light-absorbing metal nanostructures are integrated into the target tissue to facilitate selective photothermal effects. These nanostructures include gold nanorods (NRs)[22], nanocages[21], and "core/shell" structures[15−17,20]. One should be cautioned, however, that sometimes the acclaimed "core/shell" structures turn out to be aggregates of nanoparticles[33]. In any case, one of the major challenges in using metal nanostructures for PTA is their efficient *in vivo* delivery to the target sites after systemic administration[24].

To date, the success with PTA based on metal nanostructures as the photothermal coupling agents has been somewhat limited, due to the lack of suitable metal nanostructures that can satisfy several critical requirements simultaneously: i) small size, ii) spherical or near spherical shape, and iii) strong, narrow, and tunable, near-IR absorption[34,35]. Small size is important since there is an optimal size range for intracellular uptake, *e.g.*, about 40 nm for gold nanoparticles[36]. Spherical shape is generally more desirable for delivery because it minimizes friction. Strong absorption is clearly important for PTA, since it is based on heat generation resulting directly from light absorption. Narrow SPR band is desired since the light used for PTA is often narrow in frequency, and a narrow absorption band that closely matches the light frequency makes the photothermal conversion process more efficient. Tunable surface plasmon resonance (SPR) absorption is useful for matching the selected laser wavelength and minimizing tissue absorption in the NIR.

Almost all nanostructures used in PTA reported thus far can meet some of these requirements, but not all at the same time. For example, nanocages/nanocubes and nanorods can afford strong, NIR absorption, but tend to exhibit broad SPR and non-spherical shape. Likewise, aggregates of nanoparticles or "core/shells" composed essentially of aggregates, have strong NIR absorption but broad SPR and non-spherical shape. Other problems with aggregates or similar systems include structural instability and typically large size (> 100 nm). Finally, while solid spherical nanoparticles have the desired spherical shape, they exhibit weak absorption in the NIR and limited wavelength tenability[34,35]. Therefore, while a number of metal nanostructures have been investigated for PTA and similar purposes[15−17,20−22], most of them do not meet all the desired criteria simultaneously, in terms of size, shape, and absorption (wavelength and

bandwidth). Very recently, a second generation metal nanostructure has been developed, namely hollow gold nanospheres (HGNs), which have been successfully demonstrated to meet all the requirements for PTA simultaneously[23,24].

In the following, we will first briefly discuss the principle behind PTA and then provide some illustrations using different metal nanostructures. Comparison and contrast will be made whenever appropriate and possible. Since this is a fast evolving and relatively new area of research, some of the results are preliminary and interpretations tentative. It is our hope that further interest will be stimulated and research conducted in PTA in the future.

2 Principle of PTA based on metal nanostructures

The basic idea behind PTA is illustrated in Figure 1. Metal nanostructures, such as hollow gold nanospheres (HGNs)[34,37], are brought to the cancer cell through targeted interaction, *e.g.*, antibody-antigen or hormone-receptor. Light illumination of the metal nanostructures produces heat that can be used to image and destroy cancer cells. For PTA to be effective, the metal nanostructure needs to have strong light absorption at the wavelength used for treatment, usually in the NIR region for deep tissue penetration.

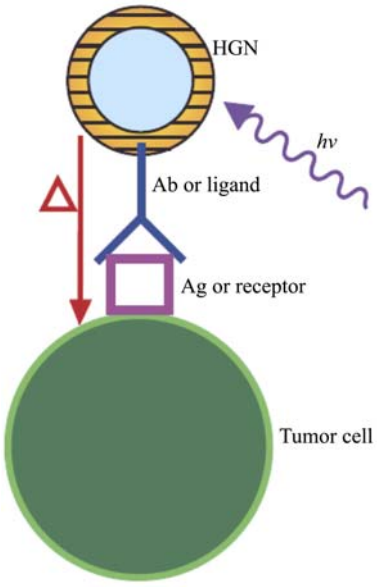

Figure 1 Illustration of the basic idea behind PTA. HGNs are actively linked to target cancer cells through antibody (Ab)-Antigen (Ag) or ligand (e.g., hormone)-receptor interaction. Heat generated from light illumination of the HGNs is used for imaging and/or destroying the cancer cells.

The damaging mechanism behind PTA is not yet well understood. Explanations proposed for heat-induced cell death from previous studies include heat shock of proteins, inactivation of membrane proteins and mitochondria, depolymerization of cytoskeletal filaments, membrane blebbing, and plasma membrane disruption due to cavitation effect[38−41]. The cavitation effect is also suggested to be responsible for bubble formation[41−43]. The gradient for cavitation-induced heating has been found to decline sharply from the epicenter, such that direct thermolysis would be limited to targeted cells near the sites of photothermal conversion[41]. Further research is clearly needed to gain a deeper understanding of the molecular mechanism of PTA. One interesting question is the local temperature on the nanostructure surface that is likely much higher than the average temperature measured with a thermometer. Molecules with temperature-dependent luminescence or Raman scattering based on the ratio of Stokes and anti-Stokes scattering may be possible methods for probing the local temperature, which are yet to be explored. It can be anticipated that the distance between the metal nanostructure and the cancer cell is an important parameter. Likewise, the location of the nanostructures in the cancer cell will also be critical, e.g., on the surface, in the membrane, or near the cell nuclei.

3 PTA based on spherical nanoparticles

Solid spherical metal nanoparticles, e.g., gold, are the simplest and most commonly used for PTA. Previous studies on laser nano-thermolysis of cancerous cells have demonstrated efficacy and specificity of malignant cell damage[5]. Damage to normal cells in the course of the laser thermolysis was not totally avoided due to less than optimal cancer cell targeting with nanoparticles. One strategy to increase efficiency of targeting involves a two-stage method: (1) formation of clusters of light-absorbing gold NPs selectively in target cells, and (2) the cell damage through laser-induced generation of vapor bubbles around NP clusters[5].

For example, experimental investigation of laser nano-thermolysis of leukemia cells was performed using 30 nm spherical gold nanoparticles as a light absorbing agent, and photothermal and fluorescent microscopies as well as flow cytometry as methods to monitor microbubble formation and resulting damage of leukemia cells in human bone marrow specimens. Figure 2 presents typical

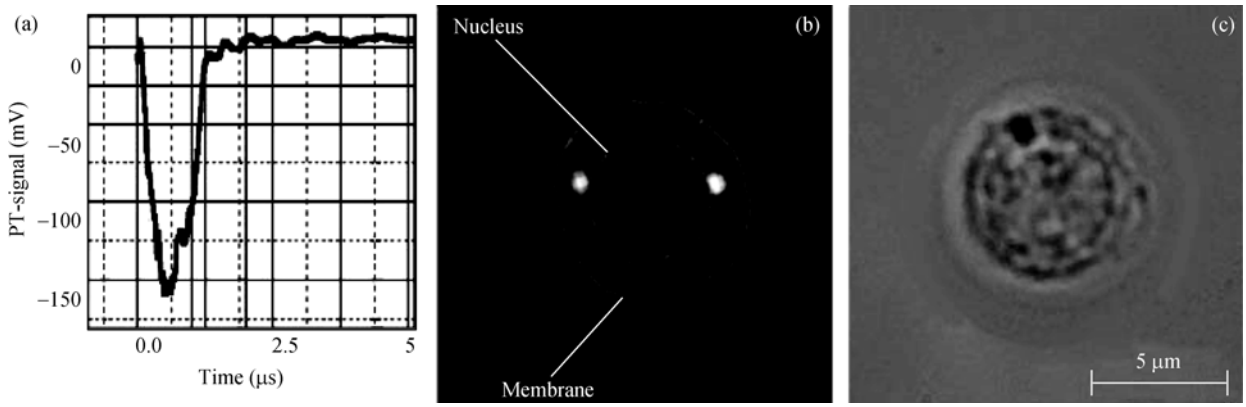

Figure 2 Typical bubble-specific PT response (a), PT-image (b), and optical image of the same cell before irradiation (c) obtained for a tumor cell after single laser pulse for the incubation conditions being 378℃, 2 hours. Reproduced from ref. [5].

bubble-specific PT response (a), PT-image (b), and optical image of the same cell before irradiation (c) obtained for a tumor cell after single laser pulse for the incubation conditions being 378℃, 2 hours.

It has been shown that the damaging effect of the bubble is localized within the cell at the origin of bubble generation while surrounding cells are not damaged[5]. This feature provides a mechanism for localized, individual cell damage. This is especially useful for situation where a small number of target cells are present among a large number of normal cells. In addition, it has been found that a few tumor cells left after laser treatment can cause new tumors[5]. Cell killing through bubble-induced lysis and necrosis seems to be dependent upon NP clustering and laser radiation properties but independent on the properties of specific cells.

It has been demonstrated that clustering of NPs, bubble generation and cell damage can be diagnosis specific[5]. The two-stage cell targeting method enables effective formation of clusters of NPs, which serve as nucleation centers for laser-induced vapor bubbles. Large NP clusters with dimensions exceeding 200 nm can be formed selectively in target, diagnosis-specific tumor cells. Laser-induced microbubbles around NP clusters can destroy individual target cells, while leaving surrounding normal cells unaffected. Laser fluence threshold of the bubble generation was found to be the lowest for the largest NP clusters and decrease with increasing cluster size. Target cells can be killed with a single laser pulse; and immediate damage of >99% human leukemia cells was achieved while 49%—87% of normal bone marrow cells survived[5].

In general, the NPs may get into the cells through specific and non-specific mechanisms. It is not possible to exclude non-specific mechanism such as phagocytosis. Therefore, efforts have been made to create nanostructures that are highly specific for target tumor cells and would not emerge in normal cells[5]. The solution is clustering of NPs that offers advantages over single NP by allowing significant decrease of optical energy required for bubble generation and bigger bubble formation.

Figure 3 shows a block diagram of the experimental protocol for laser-activated nano-thermolysis as cell elimination technology (LANTCET) and serves to illustrate the ideal behind the NP clustering approach[5]. The first stage of this approach provides accumulation of NPs at cell membrane due to receptor-MAB1-MAB2 interactions (MAB for monoclonal antibodies). The second stage involves formation of NP clusters through endocytosis of NPs. Endocytosis is a universal and fast biological process that delivers NPs or small clusters of NPs from the cell membrane into the cytoplasm where they are concentrated into larger clusters inside endosomes. The two-stage mechanism of NP targeting has been found to be rather universal and can be applied to the different types of cells (not only tumor cells). It can be regulated through the control of cell incubation parameters, time and temperature, of each stage. This mechanism employs two biological processes, endocytosis and MAB-receptor interaction, and gold NPs that do not affect cell viability[5].

A similar study has found that abnormal cells containing gold nanoparticles could be destroyed by laser thermal explosion[44]. Threshold density of a single laser pulse for thermal explosion of single gold nanosphere was 40 mJ/cm^2 and such laser density did no harm to

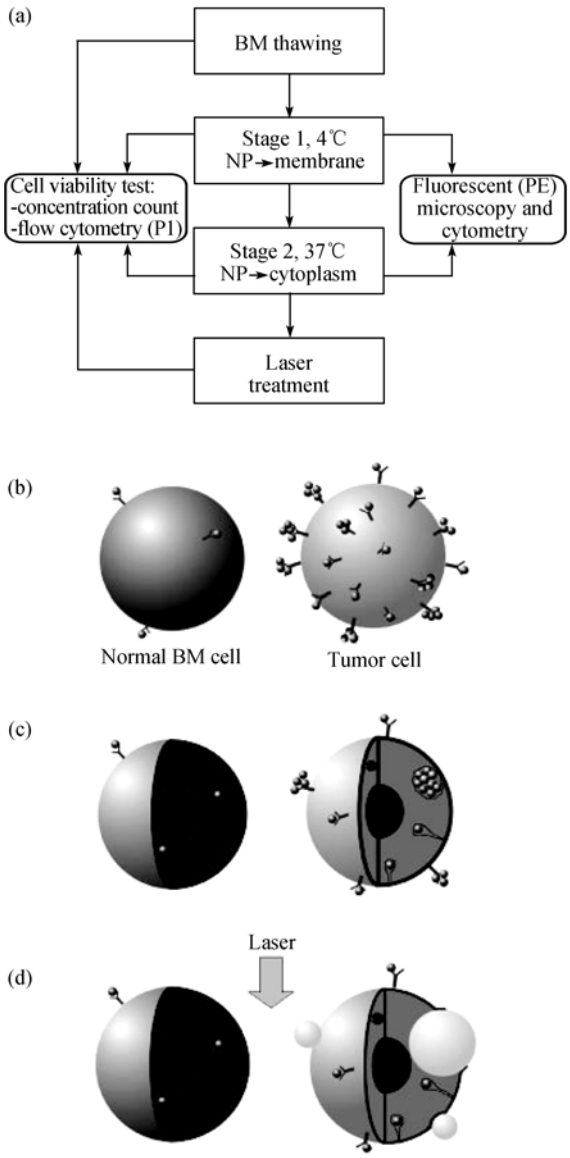

Figure 3 Block diagram of the experimental protocol for LANTCET (a) and illustration of the different steps of LANTCET: (b) membrane targeting with NPs—stage 1, (c) clustering of NPs—stage 2, (d) laser-induced vapor bubbles and cell damage. BM is for bone marrow. Reproduced from ref. [5].

healthy cells.

In another study, it has also been shown that aggregated gold nanoparticles could decrease the use of laser energy and increase the efficiency of cancer cell destruction[45]. The gold nanoparticles were conjugated to anti-epidermal growth factor receptor (anti-EGFR) antibodies for targeting the HSC 3 cancer cells (human oral squamous cell carcinoma) and illuminated with short femtosecond NIR laser pulses. Twenty-fold lower laser power threshold has been found for the photothermal destruction of cells with the gold NPs than that required to destroy the cells without nanoparticles. It was suggested that aggregated nanospheres are responsible for enhanced photothermal destruction of the cells. A quadratic dependence on the laser power for the number of destroyed cells indicated a possible second harmonic generation or a two photon absorption process[45].

While isolated NPs are easy to synthesize and have spherical shape for convenient delivery, they usually have weak NIR absorption. NIR absorption can be enhanced upon aggregation of NPs[33,46], however, the aggregates tend to have broad SPR due to inhomogeneous broadening in size and shape as well as large and non-spherical shape that are not suitable for delivery[47].

4 PTA based on nanorods

Another interesting class of nanostructures used for cancer PTA treatment is nanorods. Metal nanorods have two SPR bands, transverse at short wavelength, near 520 nm, and longitudinal at longer wavelength in the red and NIR[35]. As mentioned above, the NIR band is particularly interesting for optimal tissue penetration. The strong absorption in the NIR is expected to lead to efficient photothermal conversion upon NIR light illumination. Nanorods have been considered as effective contrast agents for *in vivo* bioimaging as well as for PTA[48].

For example, experimental studies of photothermal conversion of gold nanorod (AuNR) conversion, in conjunction with tissue-like phantoms and Monte Carlo simulation, show that the fluence threshold for AuNR conversion was in the range of 20—43 mJ/cm^2. It was demonstrated that PTA with AuNR could be effective for tumors within 10 mm of the surface of the illuminated tissue[49].

Another investigation made use of a combination of the high absorption efficiency of Au-Ag nanorods (NRs) and the target specificity of molecular aptamers[50]. This combination of Au-Ag NRs requires only 8.5×10^4 W/m^2 laser exposure to induce 93% cell death of NR-aptamer-labeled cells, as compared with most other nanomaterials (such as gold nanoshells or NRs) which require a relatively high power of laser irradiation (1×10^5—1×10^{10} W/m^2). Moreover, the aptamers have been made from cell-SELEX (systematic evolution of ligands by exponential enrichment) process. The significant advantage over other targeted therapies is that the prior knowledge of the biomarkers for the cell is not required. Additionally, this aptamer conjugates have excellent hyperthermia efficiency and selectivity with both cell

suspensions and solid tumor samples. About 50% of target (CEM) cells were severely damaged, while more than 87% of control (NB-4) cells remained intact in a suspension cell mixture[50].

As another example on the use of NRs for PTA, polyethylene glycol (PEG)-protected gold nanorods (NR), denoted as PEG-NR, have been reported to exhibit superior spectral bandwidth, photothermal heat generation per gram of gold, and circulation half-life *in vivo* ($t_{1/2}$, approximately 17 hours) compared with the prototypical tunable plasmonic particles, gold nanoshells, as well as approximately 2-fold higher X-ray absorption than a clinical iodine contrast agent[51]. After intratumoral or i.v. administration, PEG-NR biodistribution data have been derived via noninvasive X-ray computed tomography or *ex vivo* spectrometry, respectively, with computational heat transport modeling to predict photothermal heating during irradiation. Pilot therapeutic studies show that a single i.v. injection of PEG-NRs enabled destruction of all irradiated human xenograft tumors in mice[51].

Gold NRs have also been investigated for the ablation of various cancer types using both direct injection and systemic delivery. For example, PTA of colon cancer in an animal model using intravenously delivered gold nanorods has been reported[52]. Nanorods with an aspect ratio of ~3.2 and an extinction peak of 774 nm were PEGylated, suspended in an isotonic solution, and infused into the tail vein of BALB/c mice bearing subcutaneous CT26.wt murine colon cancer tumors. After 24 h, an isotropic laser fiber was inserted through a small incision in the skin to a point proximate to and beneath the tumor. The area was illuminated with 3.5 W average power for 3 minutes. The survival of the animals receiving nanorod-based PTA was statistically longer than that of the control groups with >44% complete response. Other effort has been made to develop an integrated system for photothermal tumor therapy involving the synthesis of long-circulating gold NRs as efficient NIR-"nanoantennas", biodistribution data acquisition via X-ray CT nanomaterial imaging or *ex vivo* spectrometry, and photothermal computational modeling to guide surgical irradiation planning[51]. The efficacy of a nanoantenna for photothermal therapy has been found to depend on both intrinsic and extrinsic material characteristics, as well as external parameters, such as the use of optimized dosing and irradiation protocols for effective treatment. As shown in Figure 4, spectral and photothermal properties of highly absorbing gold NRs are

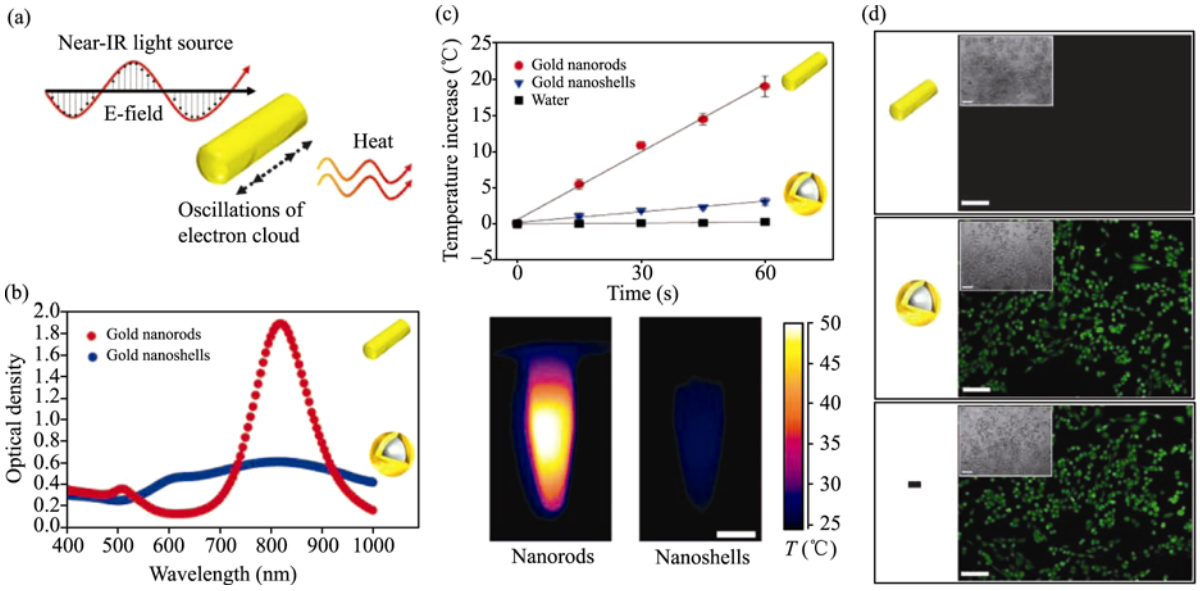

Figure 4 Spectral and photothermal properties of highly absorbing gold NRs compared with gold nanoshells. (a) schematic of photothermal heating of gold NRs. The dimensions of gold NRs are tuned to have a NIR plasmon resonance, at which point nanoparticle electrons resonantly oscillate and dissipate energy as heat. (b) spectra for PEG-gold NRs (red) and PEG-gold nanoshells (blue), a benchmark for tunable plasmonic nanomaterials, at equal gold concentrations. (c) top, rate of temperature increase for triplicate PEG-NR and PEG-gold nanoshell solutions (7 μg Au/mL, 810 nm laser, 2 W/cm^2, n=3 each); bottom, IR thermographic image of PEG-NRs versus PEG-gold nanoshells after 2 min of irradiation; scale bar, 5 mm. (d) *in vitro* photothermal toxicity of PEG-NRs over human cancer cells in culture (MDA-MB-435). Tumor cells were incubated with PEG-NRs (14 μg/mL; top), PEG-nanoshells (14 μg/mL; middle), or media alone (bottom) and treated with laser irradiation (2 W/cm^2, 810 nm, 5 min). Calcein AM staining indicates destruction of cells with PEG-NRs, whereas cells irradiated in the presence of nanoshells or media remained viable. Phase region of calcein staining is shown in inset. Scale bar, 10 μm. Reproduced from ref. [51].

more suitable for PTA than for gold nanoshells. For example, optical density of nanorods is almost 4 folds higher than for nanoshells in the NIR, and the temperature increased almost 8 folds higher with nanorods than with nanoshells. Also, higher photothermal toxicity for human cancer cells in culture (MDA-MB-435) has been found with nanorods.

Photothermal destruction of human tumors in mice using long-circulating gold NRs shown in Figure 5 demonstrated complete destruction of tumor and no evidence of tumor regrowth[51]. There were no such results with NRs alone, laser light alone or Laser light plus saline. Also time of surviving in this group has been significantly longer.

In addition, NRs could also be conjugated to molecules to facilitate delivery to tumor. For example, gold NRs have been synthesized and conjugated to anti-epidermal growth factor receptor (anti-EGFR) monoclonal antibodies and incubated in cell cultures with a nonmalignant epithelial cell line (HaCat) and two malignant oral epithelial cell lines (HOC 313 clone 8 and HSC 3)[53]. The anti-EGFR antibody-conjugated nanorods bind specifically to the surface of the malignant-type cells with a much higher affinity due to the overexpressed EGFR on the cytoplasmic membrane of the malignant cells. As a result of the strongly scattered red light from gold nano-

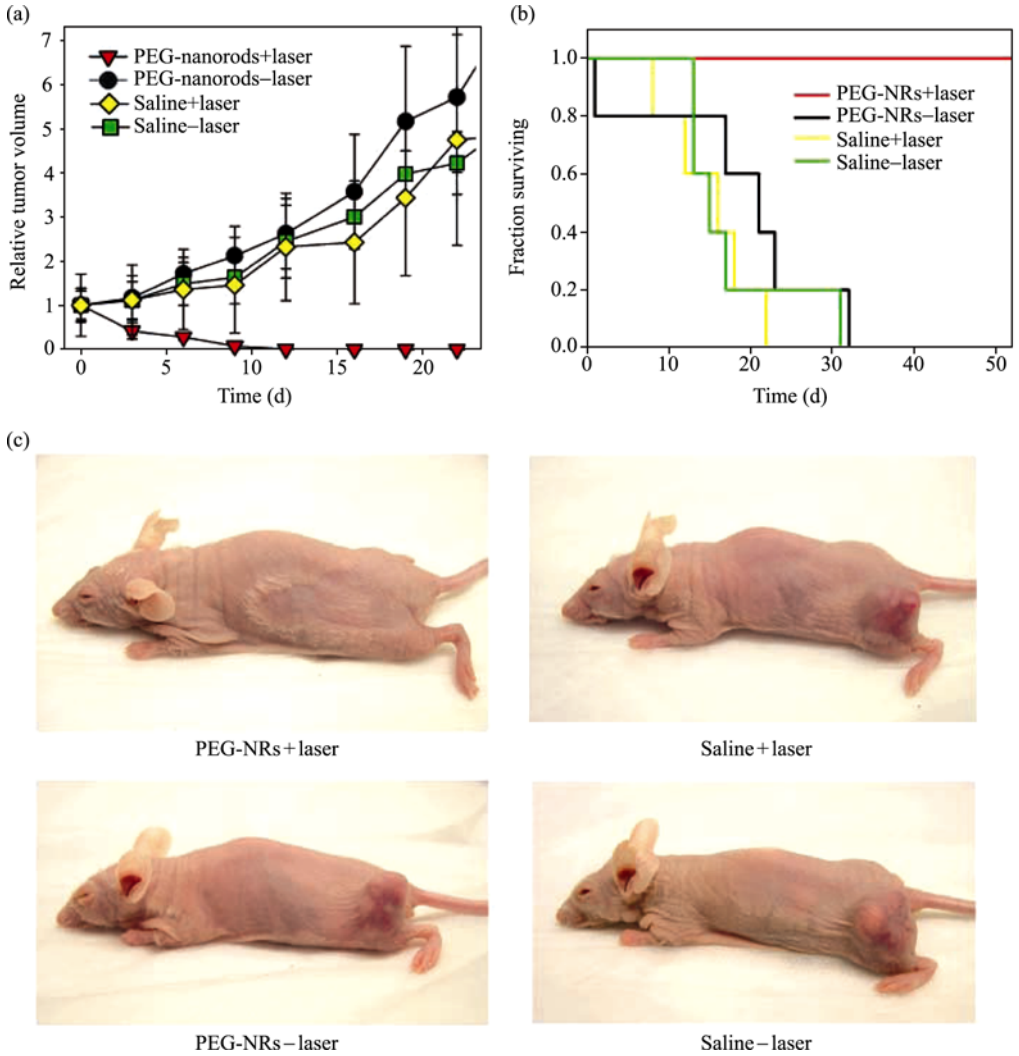

Figure 5 Photothermal destruction of human tumors in mice using long-circulating gold NRs. (a) mice harboring two MDA-MB-435 human tumors on opposite flanks were injected with either saline or PEG-NRs. After PEG-NRs had been cleared from circulation (72 h after injection), the right flank of each mouse was exposed to the computationally designed irradiation regimen (810 nm, 2 W/cm^2, 5 min). Volumetric changes in tumor sizes are plotted over time after irradiation. (b) mice harboring one MDA-MB-435 human tumor were injected with either saline or PEG-NRs and irradiated as in (a). Survival of mice after irradiation is plotted versus time after irradiation. (c) at 20 days after irradiation, NIR-irradiated, all PEG-NR–injected mice showed only a minor scar and no evidence of tumor regrowth whereas all other treatment groups harbored thriving tumors. Reproduced from ref. [51].

rods in dark field, the malignant cells could be clearly visualized and diagnosed from the nonmalignant cells. It was found that, after exposure to continuous red laser at 800 nm, malignant cells required about half the laser energy to be photothermally destroyed than the nonmalignant cells. Thus, both efficient cancer cell diagnostics and selective photothermal therapy were realized simultaneously.

Similarly, multifunctional nanoparticles, each composed of a single, amine-modified gold nanorod, decorated with multiple "pearls" of Fe_3O_4 nanoparticles capped with carboxy groups, have been prepared, and their effectiveness in simultaneous targeting, dual-mode imaging, and photothermal ablation of breast cancer cells has been demonstrated[54].

While nanorods can easily afford strong near IR absorption desired for PTA, the rod-like non-spherical shape is generally not ideal for delivery or membrane penetration. Also, their SPR spectral features tend to be broad due to two plamson bands and each is sensitive to structural heterogeneity.

5 PTA based on nanocages

Gold nanocages represent another interesting class of biocompatible metal nanostructures with potential applications in drug delivery, tumor/tissue imaging and photothermal therapy[21]. Gold nanocages can be prepared through a galvanic-replacement reaction between Ag nanostructures and $HAuCl_4$. By controlling the amount of $HAuCl_4$ added, one can tune the surface-plasmon resonance peaks of the Au nanocages into the near-infrared. The optical properties of Au nanocages for use as contrast agents in optical coherence tomography and as transducers for the selective photothermal ablation of cancer cells have been tailored. The results showed improved optical coherence tomography image contrast when Au nanocages are added to tissue phantoms. Also the selective photothermal destruction of breast cancer cells *in vitro* has been detected when immunotargeted Au nanocages were been used[21].

While encouraging, nanocages with non-spherical shape and broad SPR due to multiple dipolar modes possible may not be the most ideal metal nanostructures for PTA since the non-spherical shape is not preferred for delivery and the broad spectral will reduce photothermal conversion efficiency.

6 PTA based on "nanoshells"

The so-called "nanoshells", nanostructures with a spherical dielectric core and an outer metal shell, have been a system of interest for PTA and other applications for many years[55]. The attraction is mainly in the possibility to manipulate the optical properties by controlling the shell thickness and diameter[56]. While this is a good and simple idea in principle, its realization in practice has not been easy. Many attempts to synthesize "nanoshells" ended up with other structures, often aggregates. This has also been the origin of some debates in the literature[33,46,57]. Therefore, one must be careful when evaluating the literature about whether the acclaimed "nanoshells" are real or not. The correct establishment of the detailed structure of nanomaterials requires high quality structural characterization, e.g., high resolution transmission electron microscopy (HRTEM) or related techniques[58]. Optical spectroscopy is usually not sufficient to unambiguously determine the structure of nanomaterials[59].

With this caution in mind, early studies using acclaimed "nanoshells" (even though likely aggregates in many cases) have laid a good foundation for PTA research. For example, "nanoshells" have been designed to have both absorption and scattering properties in the NIR to provide optical contrast for improved diagnostic imaging and, at higher light intensity, rapid heating for photothermal therapy[19]. They have been demonstrated to show dramatic increase in contrast enhancement for optical coherence tomography (OCT) as well as effecttiveness in PTA[55].

A pilot study has demonstrated the passive delivery of nanoshells to an orthotopic tumor where they induced a local, confined therapeutic response and resulted in PTA of canine transmissible venereal tumor (cTVT) in a canine brain model[60]. cTVT fragments grown in severe combined immunodeficient mice were successfully inoculated in the parietal lobe of immunosuppressed, mixed-breed hound dogs without harming the normal tissues. A single dose of NIR–absorbing, 150-nm nanoshells was infused i.v. and allowed to passively accumulate in the intracranial tumors. The accumulation of nanoshells within the intracranial cTVT suggested that its neovasculature represented an interruption of the normal blood-brain barrier. Tumors were thermally ablated by percutaneous NIR radiation at 808 nm that

selectively elevated the temperature of tumor tissue. The laser dose was designed to minimize thermal damage to normal brain tissue in the absence of nanoshells and compensate for variability in the accumulation of nanoshells in tumor. Postmortem histopathology of treated brain sections showed the effectiveness and selectivity of the nanoshell-assisted thermal ablation[60].

Figure 6 shows the results of AuroLase laser treatment for cTVT in the brain of one of the dogs with nanoshells[60]. It has been shown that the normal brain tissue was intact while damage from laser irradiation had been done only to the tumor. Complete thermal ablation of the inferior lobe of the tumor was found.

In addition, selective targeting of PC-3 cells with nanoshells conjugated to ephrinA I, a ligand for EphA2 receptor overexpressed on PC-3 cells, has been investigated[60]. Selective photothermal destruction of these cells upon application of the NIR laser has been demonstrated. Figure 7 shows EA of gold content in cTVT and normal canine white matter. It was found that nanoshells accumulated more than 10 folds higher in tumor than in white matter.

In another experiment, *in vitro* studies have confirmed the ability to selectively induce cell death of breast carcinoma cells with the photothermal interaction

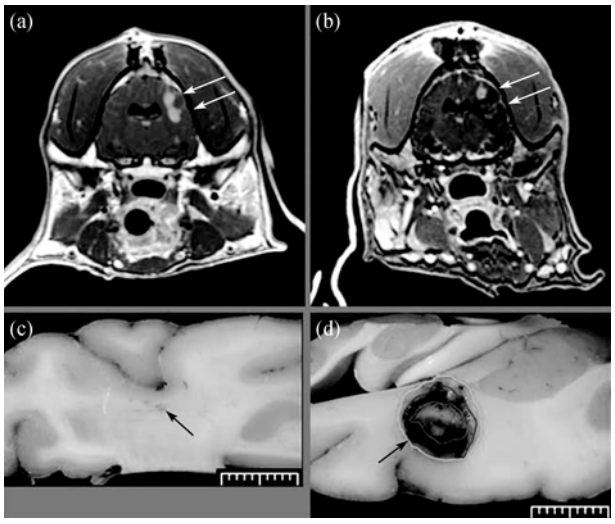

Figure 6 AuroLase treatment for cTVT in the brain of dog 4. (a) arrows, MR-DCE axial image of dog brain showing contrast enhancement of bilobed tumor along inoculation track. (b) arrows, MR-DCE axial image of dog brain after laser treatment showing ablation of inferior lobe. (c) control cerebral hemisphere showing no ablation in normal brain. Arrow, fiber insertion point. (d) ablation zones (inner ring = boundary of tumor, middle ring = boundary of thermal necrosis, outer ring = boundary of zone of edema) around nanoshell-containing tumor. Arrow, fiber insertion point. Reproduced from ref. [60].

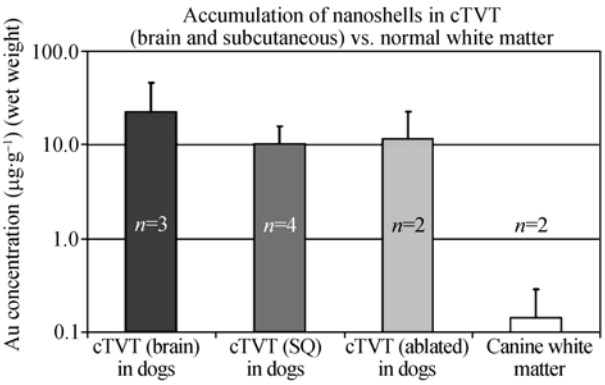

Figure 7 Elemental analysis of gold content in cTVT and normal canine white matter. Reproduced from ref. [60].

of immunonanoshells and NIR light[19]. Prior to incubation with anti-human epidermal growth factor receptor (HER2) immunonanoshells, HER2-expressing SK-BR-3 breast carcinoma cells were seeded alone or adjacent to human dermal fibroblasts (HDFs). Anti-HER2 immunonanoshells bound to HER2-expressing cells resulted in the death of SK-BR-3 cells after NIR exposure only within the irradiated area, while HDFs remained viable after similar treatment since the immunonanoshells did not bind to these cells at high levels. Control nanoshells, conjugated with nonspecific anti-IgG or PEG, did not bind to either cell type, and cells continued to be viable after treatment with these control nanoshells and NIR irradiation[61]. Figure 8 shows live and dead stain of cells incubated with nanoshells and exposed to the NIR laser with a spot size of 2 mm. It was found that bare nanoshells allowed ablation of both cell types indiscriminately while EphrinAl-nanoshells allowed ablation of only PC-3 cell line.

Nanoshell photothermal cancer therapy has been shown to work through the preferential accumulation of nanoshells in a tumor and absorption of NIR light by those particles to locally generate heat at the tumor site[62]. It has been found that nanoshells could passively accumulate in tumors after intravenous injection. It could be considered as a result of the leaky vasculature characteristic of neoplastic tumors. Application of NIR light to the tumor after systemic injection of nanoshells and their accumulation at the tumor site lead to the absorption of energy in nanoshells and their heating due to destruction of the tumor tissue which contains nanoshells. It has been demonstrated in a mouse model that nanoshell-absorbed tumors completely regressed after NIR illumination without tumor regrowth. The

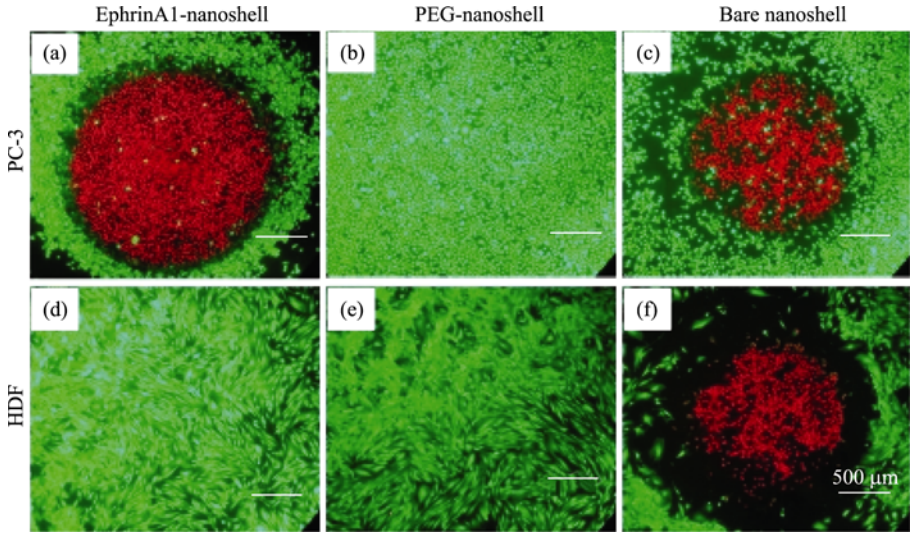

Figure 8 Live/dead stain of cells incubated with nanoshells and exposed to the NIR laser with a spot size of 2 mm. PC-3 cells were incubated with (a) EphrinAl-, (b) PEG-, and (c) bare nanoshells for 2 h and then exposed to the NIR laser in the center of the wells, and (d), (e), and (f) HDF underwent the same treatment. Note that the bare nanoshells allowed ablation of both cell types indiscriminately while EphrinAl-nanoshells allowed ablation of only PC-3 cell line. Live and dead cells are shown in green and red, respectively. Reproduced from ref. [61].

tumors containing the nanoshells underwent rapid temperature rise leading to irreversible tissue damage, while laser application to nearby healthy tissue or to tumors not treated with nanoshells did not cause a significant temperature increase[62].

Figure 9 shows two cell types, SK-BR-3 (left side of (a) and (b)) and HDF (right side of (a) and (b)) cells, grown on glass cover slip and aligned as shown prior to the experiment[62]. Anti-HER2 immunonanoshells bound to the HER2 expressing SK-BR-3 cells resulted in targeted cell death after laser irradiation (Figure 9(a)). Nanoshells coated in PEG alone did not bind cells and laser irradiation produced no area of cell death (Figure 9(b)). The results clearly show the importance and success of targeting through antibody-antigen interaction[62].

Another study of nanoshells examined the feasibility of nanoshell-assisted photothermal therapy (NAPT) based on their strong near IR absorption and the possibility of passive accumulation in the tumor[17]. Tumors were grown in immune-competent mice by subcutaneous injection of murine colon carcinoma cells (CT26.WT). Polyethylene glycol (PEG) coated nanoshells (≈130 nm diameter) with peak optical absorption in the NIR were intravenously injected and allowed to circulate for 6 h before tumors were illuminated with a diode laser (808 nm, 4 W/cm^2, 3 min). All the treated mice appeared healthy and tumor free >90 days later. Control animals and additional sham-treatment animals, e.g., laser treatment

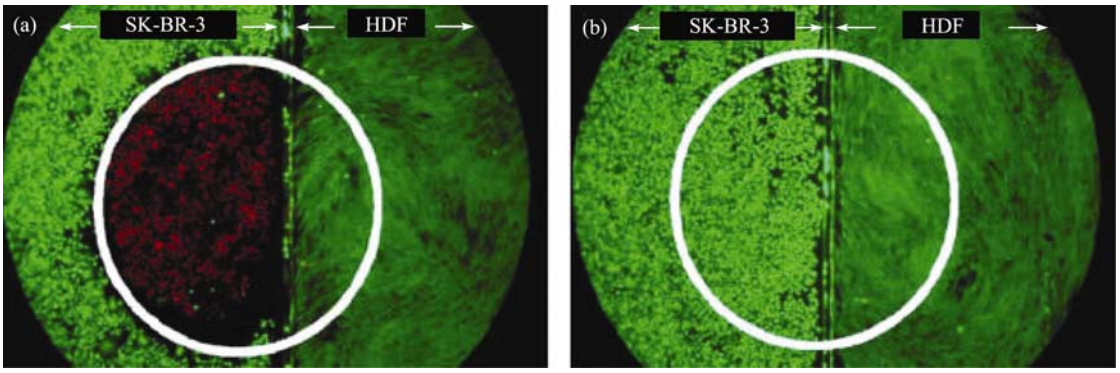

Figure 9 Two cell types, SK-BR-3 (left side of (a) and (b)) and HDF (right side of (a) and (b)) cells, were grown on glass cover slip and aligned as shown prior to the experiment. (a) Anti-HER2 immunonanoshells bound to the HER2 expressing SK-BR-3 cells resulted in targeted cell death after laser irradiation. The laser area is outlined in white. (b) Nanoshells coated in PEG alone did not bind cells and laser irradiation produced no area of cell death. Laser spot is 2.5 mm wide. Reproduced from ref. [62].

without nanoshell injection, were euthanized when tumors grew to a predetermined size, 6—19 days post-treatment[17].

A similar approach to specifically target malignant brain tumor cells for photothermal ablation using antibody-tagged, NIR-absorbing gold-silica nanoshells, referred to as immunonanoshells has been developed[63]. This study confirmed previous investigation and showed that after localized in tumor cells, these nanoshells are extremely efficient at absorbing near-infrared light. In addition, they can generate sufficient heat to kill cancer cells upon exposure to laser light. In this study the efficacy of immunonanoshells *in vitro* against both medulloblastoma and high-grade glioma cell lines has been evaluated. An antibody against HER2 to target gold-silica nanoshells to medulloblastoma cells has been used, since HER2 is frequently overexpressed in medulloblastoma. It was found that the treatment with HER2-targeted nanoshells, but not non-targeted nanoshells, followed by exposure to laser light can induce cell death in the HER2-overexpressing medulloblastoma cell line Daoy.2, as well as the parental Daoy cell line, which expresses HER2 at a moderate level, but not in dermal fibroblasts. In similar experiments, gold-silica nanoshells were conjugated to an antibody against interleukin-13 receptor-α2 (IL13Ra2), an antigen that is frequently overexpressed in gliomas[63].

While the results from "nanoshells" are encouraging due to their strong NIR absorption, it has generally been very challenging to produce true high quality nanoshells. As mentioned above, many acclaimed "nanoshells" are "shells" of aggregates[33,46,57]. Such structures are large in size (especially when a large silica particles are used as the core) and non-spherical in shape, show broad inhomogeneity in size and shape distribution, and have multiple dipolar modes and thereby board SPR absorption[34,35]. All these features are not ideal for PTA.

7 PTA based on hollow gold nanospheres

As can be seen from the examples discussed above, the use of plasmonic gold nanostructures can reduce the laser energy necessary for selective tumor cell destruction. However, the ability for targeted delivery of the nanostructures to tumor cells is limited. Recently, a new class of molecular specific photothermal coupling agents based on hollow gold nanospheres (denoted as HAuNS or HGNs) has been developed[37]. Figure 10 shows a photograph (left) and UV-vis spectra (right) of a number of HGN samples with different combinations of shell diameter and thickness that determine the peak position of the SPR absorption[37]. One can control the shell diameter and thickness to manipulate the color of the HGNs at will for different applications. For example, the HGNs with strong near IR absorption are ideally suited for PTA. In addition to the strong near IR absorption, the HGNs have small size (30—50 nm) and spherical shape, both are highly desired for delivery and membrane penetration [36].

These HGNs have been successfully demonstrated in both *in vitro* and *in vivo* PTA of carcinoma and melanoma cancer cells[23,24]. In the carcinoma PTA study, HGNs were covalently attached to monoclonal antibody directed at epidermal growth factor receptor (EGFR) overexpressed in carcinoma cancer cells[23]. The resulting anti-EGFR-HGNs exhibited excellent colloidal stability and efficient photothermal effect in the NIR region. EGFR-mediated selective uptake of anti-EGFR-HGNs in EGFR-positive A431 tumor cells but not IgG-HGNs control was shown *in vitro* by imaging scattered light from the nanoshells. Irradiation of A431 cells treated with anti-EGFR-HGNs with NIR laser resulted in selective destruction of these cells. In contrast, cells treated with anti-EGFR-HGNs alone, laser alone, or IgG-HGNs plus laser did not show observable effect on cell viability. Using ^{111}In-labeled HGNs, had been shown that anti-EGFR-HGNs could be delivered to EGFR-positive tumors at 6.8% ID/g, and the microscopic image of excised tumor with scattering signal from nanoshells confirmed preferential delivery to A431 tumor of anti-EGFR-HGNs compared with IgG-HGNs.

Figure 11 compares the light-scattering images of A431 cells incubated with C225-HGNs, IgG-HGNs, or C225-HGNs plus a large excess of C225 (blocking). Only dim greenish light was detected when cells were incubated with IgG-HGNs. This signal was due to autofluorescence and scattered light from the cell organelles in the cell cytoplasm and membrane. In contrast, C225-HGNs exhibited a strong signal in perinucleic areas in the cells. Moreover, uptake of C225-HGNs in the A431 cells was efficiently blocked by the anti-EGFR antibody C225 (Figure 3). The signal intensity from scattered light in cells treated with C225-HGNs was 10-fold higher than that in cells treated with IgG-HGNs. Similar scattering intensities were observed when cells exposed

to IgG-HGNs were compared with cells exposed to C225-HGNs plus C225.

Twenty-four hours after laser treatment, most A431 cells treated with C225-HGNs followed by NIR laser irradiation (40 W/cm2 for 5 min) were dead (lysed or stained red with EthD-1); none of the other groups (control, C225-HGNs alone, irradiation alone, and IgG-HGNs plus laser) showed observable damage to the cancer cells (Figure 12).

Radiotracer counting study also showed that C225-HGNs had a higher uptake value in the A431 tumors than did IgG-HGNs, representing a 48% gain for targeted HGNs. Significantly, there was >3-fold increase in the number of nanoshells and/or nanoshell aggregates per field observed under dark-field microscope in the perivascular area of the tumor in mice injected with C225-HGNs than in mice injected with IgG-HGNs, suggesting that the interaction between C225-HGNs and EGFR may have facilitated extravasation of the nanoshells into the interstitial space[23]. Overall, the absenceof silica core, the relatively small particle size and high tumor uptake, the absence of cytotoxic surfactant required for stabilization, and the demonstrated efficacy suggest that immuno-HGNs have excellent potential to extend to *in vivo* PTA therapy[23].

Indeed, the possibility to develop melanoma-targeted HGNs and evaluate their potential utility for selective *in vivo* PTA in melanoma has already been demonstrated successfully[24]. For this purpose, the HGNs were stabilized with polyethylene glycol (PEG) coating and attached with a melanocyte-stimulating hormone (MSH) analog, [Nle4,D-Phe7]a-MSH (NDP-MSH), which is a potent agonist of melanocortin type-1 receptor (MC1R) overexpressed in melanoma. The intracellular uptake of the NDP-MSH conjugated PEGylated HGNs (NDP-MSH-PEG-HGNs) and the distribution of h-arrestin were examined in murine B16/F10 melanoma cells. The biodistribution of NDP-MSH-PEG-HGNs was assessed at 4 hours post i.v. injection in tumor-bearing nude mice. PTA effect was evaluated both histologically using excised tissue and functionally by [18F] fluorodeoxyglucose positron emission tomography.

NDP-MSH-PEG-HGNs consist only of a thin gold wall with hollow interior (outer diameter, 43.5 F 2.3 nm; shell thickness, 3－4 nm), which displays strong and tunable resonance absorption in NIR region (peak, 808 nm). The nanoparticles were specifically taken up by melanoma cells, which initiated the recruitment of h-arrestins, the adapters to link the activated G-protein coupled receptors to clathrin, indicating the involvement of receptor-mediated endocytosis[24].

This resulted in enhanced extravasation of NDP-MSH-PEG-HGNs from tumor blood vessels and their dispersion into tumor matrix compared with nonspecific PEGylated HGNs. Successful selective photothermal ablation of B16/F10 melanoma with targeted HGNs was confirmed by histological and [18F] fluorodeoxyglucose positron emission tomography evaluation at 24 hours post near IR region laser irradiation at a low-dose energy of 30 J/cm^2 (Figure 13) These results have successfully established that NDP-MSH-PEG-HGNs have the potentials to mediate targeted PTA of melanoma.

The above *in vitro* and *in vivo* studies have shown that the HGNs are ideally suited for PTA applications because of their unique combination of spherical shape, small size (average outer diameter of 30－50 nm), absence of silica core, as well as narrow, tunable and strong absorption in the NIR region. Using a small-molecular-weight peptide as a targeting ligand and attaching it at the end of PEG chains, it had been showed, for the first time, receptor-mediated active targeting of melanoma and efficient PTA with photothermal coupling agents *in vivo*. These studies have also demonstrated that noninvasive [18F] fluorodeoxyglucose PET can be useful in monitoring early treatment response after PTA. Both size and shape have been recognized to be critical in determining cell uptake of nanostructures[36].

Much work remains to be done to advance this technology further to the level for clinical use. For example, more detailed preclinical studies with regard to excretion/clearance, safety, and efficacy of targeted HGNs need to be documented. The physicochemical properties of HGNs (including particle size and surface characteristics) may be further improved to minimize their retention in organs such as the liver, spleen, and kidney. Studies correlating intratumoral distribution of HGNs, temperature map, and thermal damage *in vivo* using noninvasive imaging techniques will be another area warranting future investigations. Recent preliminary studies have shown that the HGNs are stable up to 85℃ and study of structural integrity at higher temperature is needed. Likewise, cell toxicity and biodegradability need to be investigated for HGN and similar metal nanostructures for biomedical applications[64－67].

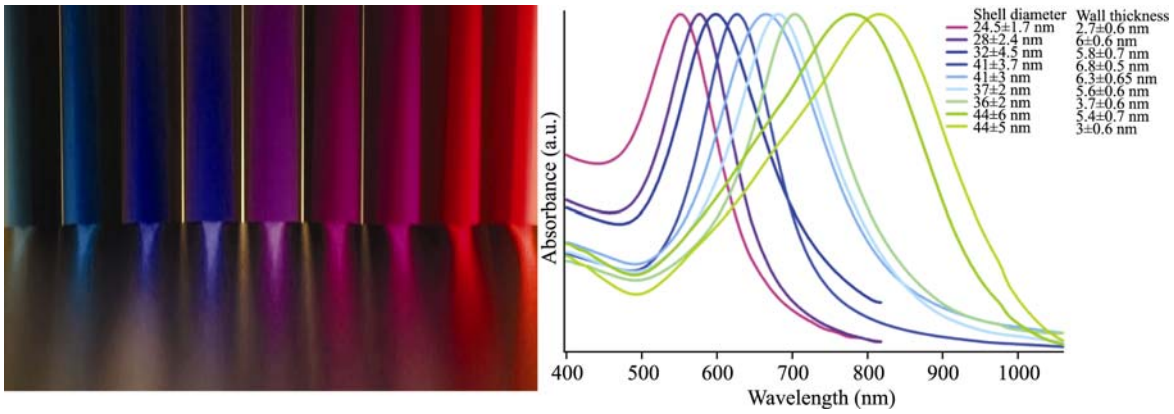

Figure 10 Photograph of hollow gold nanospheres (HGNs) of different colors (left) and UV-vis electronic absorption spectra (right). The HGNs have different combinations of shell thickness and diameter. Reproduced from ref. [37].

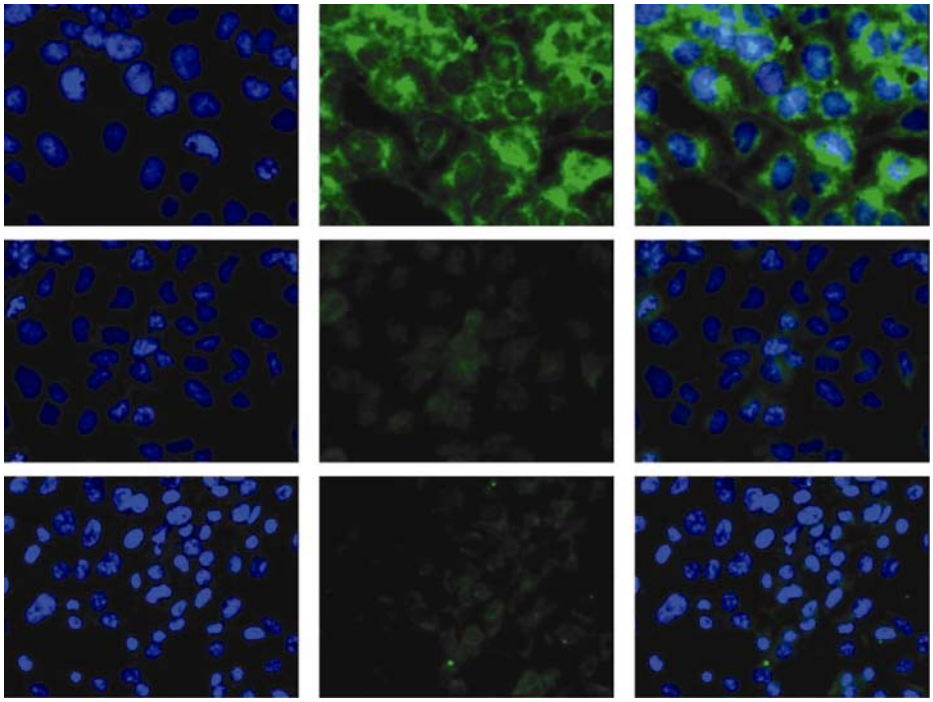

Figure 11 Selective binding of anti-EGFR-conjugated HGNs to A431 cells. A431 cells were seeded onto a 96-well plate and incubated with C225- HGNs (7.3×10^{10} particles/mL), IgG-HGNs (7.3×10^{10} particles/mL), or C225 (500 Ag/mL) plus C225-HGNs for 30 min at 37℃. Only cells incubated with C225-HAuN S had a strong light-scattering signal. Cells were stained with DAPI for visualization of cell nuclei (blue). Light-scattering images of nanoshells were pseudocolored green. Original magnification, × 630. Reproduced from ref. [23]

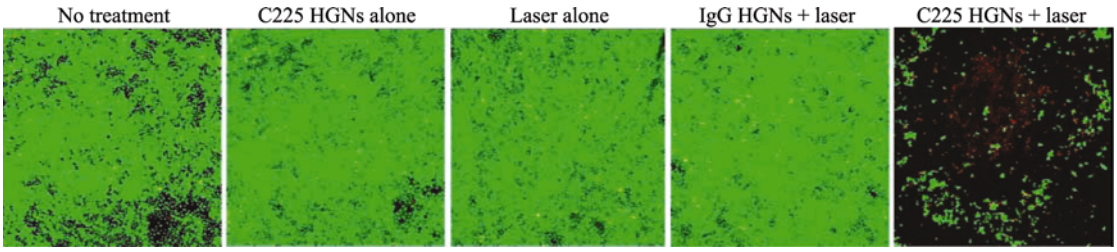

Figure 12 Cell viability after various treatments. Cells retained normal morphology with no apparent death observed (stained green with calcein CM) when cells were not treated or treated with C225-HGNs alone, NIR laser alone, or non-targeted IgG-HGNs plus NIR laser. In contrast, most cells were dead after treatment with C225-HGNs plus NIR laser. Dead cells were labeled red with Eth D-1. Magnification, ×40. Reproduced from ref. [23].

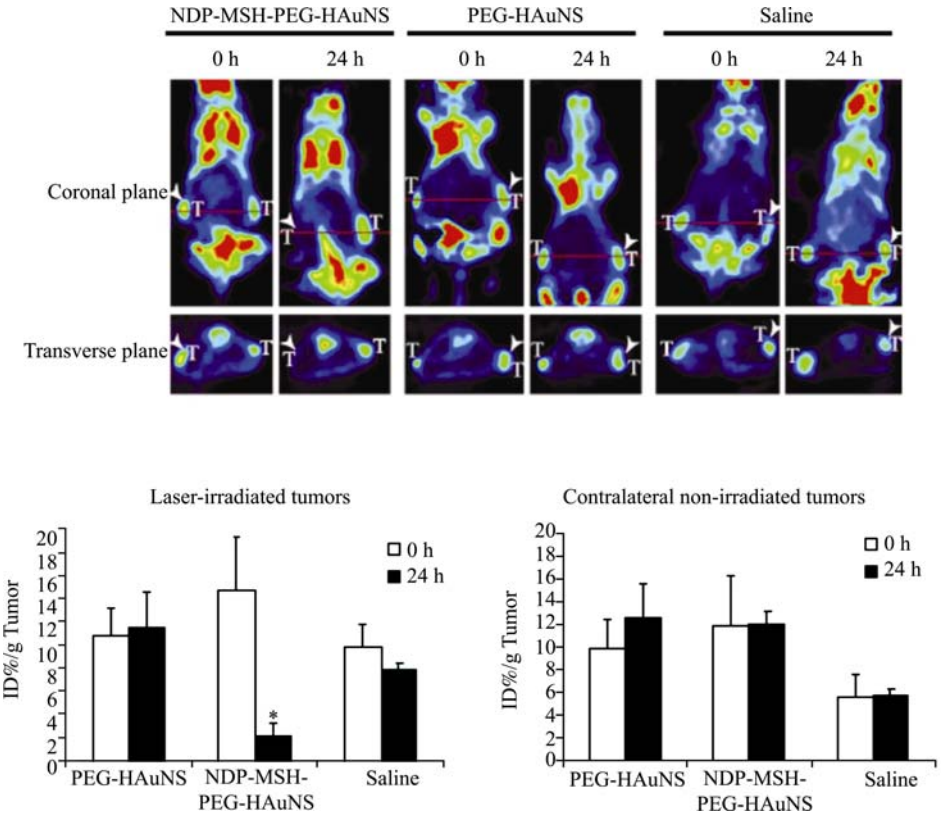

Figure 13 *In vivo* photothermal ablation with targeted NDP-MSH-PEG-HGNs induced selective destruction of B16/F10 melanoma in nude mice[24]. [^{18}F]fluorodeoxyglucose positron emission tomography (PET) imaging shows significantly reduced metabolic activity in tumors after photothermal ablation in mice that were pretreated with NDP-MSH-PEG-HGNs, but not in mice pretreated with PEG-HGNs or saline. [^{18}F]fluorodeoxyglucose PET was conducted before (0 h) and 24 h after near-IR laser irradiation (0.5 W/cm^2 at 808 nm for 1 min), which was commenced 4 h after i.v. injection of HGNs or saline (T for tumor). Arrowheads in the figure indicate tumors irradiated with near-IR light. [^{18}F]fluorodeoxyglucose uptakes (%ID/g) before and after laser treatment are shown graphically at the bottom. Bars, SD (n=3). *, $P<0.01$ for %ID/g posttreatment versus %ID/g pretreatment. HAuNS or HGNs termed in this original work is the same as HGN. Reproduced from ref. [24].

8 Concluding remarks

In summary, PTA is a promising new medical modality for diagnosis and therapeutic treatment of cancer and possibly other diseases. The use of metal nanostructures with appropriate structural and optical properties can significantly enhance the efficiency of PTA. When it is used in conjunction with active targeting based on antibody-antigen or ligand-receptor interaction, high selectivity can be achieved. Preliminary *in vitro* and *in vivo* studies of PTA therapy for cancer, such as melanoma and carcinoma, have demonstrated successfully the power and potential of PTA as a selective and efficient method for cancer therapy.

Some outstanding issues to be addressed include the fundamental mechanism behind PTA and cytotoxicity of the metal nanostructures, even though gold and silver nanomaterials are considered as biocompatible and have relatively low toxicity. Different nanostructures also need to be compared in a meaningful manner, e.g., under similar or identical experimental conditions, to determine the optical metal nanostructures for PTA. New metal nanostructures are expected to continue to be developed with the goal to achieve the highest PTA efficiency possible. Methods need to be optimized for light delivery, e.g., using optical fibers, especially when internal organs are involved. Use of other sources of radiation that can penetrate deeper into tissues than light, e.g., X-ray and radiofrequency, may also be considered as alternatives for activating the metal nanostructures for heat generation. These are just some of the possible research directions in the promising and fast-growing field of PTA for cancer treatment.

1 Torshina N L, Posypanova A M, Volkova A I. New sensitizers and rapid monitoring of their photodynamic activity. SPIE Proc, 1996, 2675: 254－255

2 Kalija O L, Meerovich G A, Torshina N L, Kogan E A, Loschenov V B, Lukyanets E A, Kogan B Y, Butenin A V, Vorozhtsov G N, Kuzmin S G, Volkova A I, Posypanova A M. Improvement of cancer PDT using sulphophthalocyanine and sodium ascorbate. SPIE Proc, 1997, 3191: 177－179

3 Jacques S L, McAuliffe D J. The melanosome: the threshold temperature for explosive vaporization and internal absorption coefficient during pulsed laser irradiation. Photochem Photobiol, 1991, 53: 769－775

4 Lin C P, Kelly N W, Sibayan S A B, Latina M A, Anderson R R. Selective cell killing by microparticle absorption of pulsed laser radiation. IEEE J Sel Top Quant, 1999, 5(4): 963－968

5 Lapotko D O, Lukianova E and Oraevsky A A. Selective laser nano-thermolysis of human leukemia cells with microbubbles generated around clusters of gold nanoparticles. Laser Surg Med, 2006, 38(6): 631－642

6 Gerstman B S, Thompson C R, Jacques S L, Rogers M E. Laser induced bubble formation in the retina. Laser Surg Med, 1996, 18(1): 10－21

7 West J L, Halas N J. Engineered nanomaterials for biophotonics applications: Improving sensing, imaging, and therapeutics. Annu Rev Biomed Eng, 2003, 5: 285－292

8 Kogan B Y, Butenin A V, Torshina N L, Kogan E A, Kaliya O L, Lukyanets E A, Luzhkov Y M, Derkacheva V M, Pankratov A A, Vorozhtsov G N, Volkova A I. Aluminium sulphophthalocyanine as an NIR photosensitizer for PDT. SPIE, 1999

9 Meerovich G A, Torshina N L, Loschenov V B, Stratonnikov A A, Volkova A I, Vorozhtsov G N, Kaliya O L, Lukyanets E A, Kogan B Y, Butenin A V, Kogan E A, Gladskikh O P, Polyakova L N. Experimental study of PDT with aluminum sulphophthalocyanine using sodium ascorbate and hyperbaric oxygenation. SPIE, 1999

10 Dougherty T J. Photodynamic therapy for treatment of cancer. J Opt Soc Am B, 1984, 1(3): 555－555

11 Xue L Y, Chiu S M, Oleinick N L. Photodynamic therapy-induced death of MCF-7 human breast cancer cells: A role for caspase-3 in the late steps of apoptosis but not for the critical lethal event. Exp Cell Res, 2001, 263(1): 145－155

12 Zuluaga M F, Lange N. Combination of photodynamic therapy with anti-cancer agents. Curr Med Chem, 2008, 15(17): 1655－1673

13 Thomsen S. Pathological analysis of photothermal and photomechanical effects of laser-tissue interactions. Photochem Photobiol, 1991, 53(6): 825－835

14 Balogh L P, Tse C, Lesniak W, Ye J, O'Donnell M, Khan M K. Photomechanical therapy: destruction of nanocomposite labeled cells by laser induced optical breakdown. Nanomed-Nanotech Bio Med, 2007, 3(4): 350－350

15 Hirsch L R, Stafford R J, Bankson J A, Sershen S R, Rivera B, Price R E, Hazle J D, Halas N J, West J L. Nanoshell-mediated near-infrared thermal therapy of tumors under magnetic resonance guidance. P Natl Acad Sci USA, 2003, 100(23): 13549－13554

16 Loo C, Lin A, Hirsch L, Lee M H, Barton J, Halas N, West J, Drezek R. Nanoshell-enabled photonics-based imaging and therapy of cancer. Tech Cancer Res Tr, 2004, 3(1): 33－40

17 ONeal D P, Hirsch L R, Halas N J, Payne J D, West J L. Photo-thermal tumor ablation in mice using near infrared-absorbing nanoparticles. Cancer Lett, 2004, 209(2): 171－176

18 Camerin M, Rello S, Villanueva A, Ping X Z, Kenney M E, Rodgers M A J, Jori G. Photothermal sensitisation as a novel therapeutic approach for tumours: Studies at the cellular and animal level. Eur J Cancer, 2005, 41(8): 1203－1212

19 Gobin A M, Lee M H, Halas N J, James W D, Drezek R A, West J L. Near-infrared resonant nanoshells for combined optical imaging and photothermal cancer therapy. Nano Lett, 2007, 7(7): 1929－1934

20 Ji X J, Shao R P, Elliott A M, Stafford R J, Esparza-Coss E, Bankson J A, Liang G, Luo Z P, Park K, Markert J T, Li C. Bifunctional gold nanoshells with a superparamagnetic iron oxide-silica core suitable for both MR imaging and photothermal therapy. J Phys Chem C, 2007, 111(17): 6245－6251

21 Skrabalak S E, Au L, Lu X M, Li X D, Xia Y N. Gold nanocages for cancer detection and treatment. Nanomedicine, 2007, 2(5): 657－668

22 Huang X H, El-Sayed I H, Qian W, El-Sayed M A. Cancer cells assemble and align gold nanorods conjugated to antibodies to produce highly enhanced, sharp, and polarized surface Raman spectra: A potential cancer diagnostic marker. Nano Lett, 2007, 7(6): 1591－1597

23 Melancon M P, Lu W, Yang Z, Zhang R, Cheng Z, Elliot A M, Stafford J, Olson T, Zhang J Z, Li C. *In vitro* and *in vivo* targeting of hollow gold nanoshells directed at epidermal growth factor receptor for photothermal ablation therapy. Mol Cancer Therapeut, 2008, 7(6): 1730－1739

24 Lu W, Xiong C Y, Zhang G D, Huang Q, Zhang R, Zhang J Z, Li C. Targeted photothermal ablation of murine melanomas with melanocyte-stimulating hormone analog-conjugated hollow gold nanospheres. Clin Cancer Res, 2009, 15(3): 876－886

25 Paltauf G, Dyer P E. Photomechanical processes and effects in ablation. Chem Rev, 2003, 103(2): 487－518

26 Jain P K, Huang X H, El-Sayed I H, El-Sayed M A. Noble metals on the nanoscale: Optical and photothermal properties and some applications in imaging, sensing, biology, and medicine. Accounts Chem Res, 2008, 41(12): 1578－1586

27 Chakravarty P, Marches R, Zimmerman N S, Swafford A D E, Bajaj P, Musselman I H, Pantano P, Draper R K, Vitetta E S. Thermal ablation of tumor cells with anti body-functionalized single-walled carbon nanotubes. P Natl Acad Sci USA, 2008, 105(25): 8697－8702

28 Arayne M S, Sultana N. Nanoparticles in drug delivery for the treatment of cancer. Pak J Pharm Sci, 19(3): 2006, 258－268
29 Ambrogi M C, Fontanini G, Cioni R, Faviana P, Fanucchi O, Mussi A. Biologic effects of radiofrequency thermal ablation on non-small cell lung cancer: Results of a pilot study. J Thorac Cardiov Sur, 2006, 131(5): 1002－1006
30 Stern J M, Stanfield J, Kabbani W, Hsieh J T, Cadeddu J R A. Selective prostate cancer thermal ablation with laser activated gold nanoshells. J Urology, 2008, 179(2): 748－753
31 Boaz T L, Lewin J S, Chung Y C, Duerk J L, Clampitt M E, Haaga J R. MR monitoring of MR-guided radiofrequency thermal ablation of normal liver in an animal model. J Magn Reson Imaging, 1998, 8(1): 64－69
32 Nguyen C T, Campbell S C. Salvage of local recurrence after primary thermal ablation for small renal masses. Exp Rev Anticancer Ther, 2008, 8(12): 1899－1905
33 Schwartzberg A M, Grant C D, van Buuren T, Zhang J Z. Reduction of HAuCl4 by Na2S revisited: The case for Au nanoparticle aggregates and against Au2S/Au Core/Shell particles. J Phys Chem C, 2007, 111(25): 8892－8901
34 Schwartzberg A M, Zhang J Z. Novel optical properties and emerging applications of metal nanostructures. J Phys Chem C, 2008, 112: 10323－10337
35 Zhang J Z, Noguez C. Plasmonic optical properties and applications of metal nanomaterials. Plasmonics, 2008, 3(4): 127－150
36 Chithrani B D, Ghazani A A, Chan W C W. Determining the size and shape dependence of gold nanoparticle uptake into mammalian cells. Nano Lett, 2006, 6(4): 662－668
37 Schwartzberg A M, Olson T Y, Talley C E, Zhang J Z. Synthesis, characterization, and tunable optical properties of hollow gold nanospheres. J Phys Chem B, 2006, 110(40): 19935－19944
38 Bowler K, Laudien H, Laudien I. Cellular heat injury. J Therm Biol, 1983, 8(4): 426－430
39 Bass H, Coakley W T, Moore J L, Tilley D. Hyperthermia-induced changes in the morphology of CHO-K1 and their refractile inclusions. J Therm Biol, 1982, 7(4): 231－242
40 Wust P, Hildebrandt B, Sreenivasa G, Rau B, Gellermann J, Riess H, Felix R, Schlag P M. Hyperthermia in combined treatment of cancer. Lancet Oncol, 2002, 3(8): 487－497
41 Tong L, Zhao Y, Huff T B, Hansen M N, Wei A, Cheng J X. Gold nanorods mediate tumor cell death by compromising membrane integrity. Adv Mater, 2007, 19(20): 3136－3141
42 Kotaidis V, Plech A. Cavitation dynamics on the nanoscale. Appl Phys Lett, 2005, 87(21): 213102－213104
43 Zharov V P, Galitovskaya E N, Johnson C, Kelly T. Synergistic enhancement of selective nanophotothermolysis with gold nanoclusters: Potential for cancer therapy. Laser Surg Med, 2005, 37(3): 219－226
44 Letfullin R R, Joenathan C, George T F, Zharov V P. Laser-induced explosion of gold nanoparticles: potential role for nanophotothermolysis of cancer. Nanomedicine, 2006, 1(4): 473－480
45 Huang X, Qian W, El-Sayed I H, El-Sayed M A. The potential use of the enhanced nonlinear properties of gold nanospheres in photothermal cancer therapy. Laser Surg Med, 2007, 39(9): 747－753
46 Norman T J, Grant C D, Magana D, Zhang J Z, Liu J, Cao D L, Bridges F, van Buuren A. Near infrared optical absorption of gold nanoparticle aggregates. J Phys Chem B, 2002, 106(28): 7005－7012
47 Grant C D, Schwartzberg A M, Norman T J, Zhang J Z. Ultrafast electronic relaxation and coherent vibrational oscillation of strongly coupled gold nanoparticle aggregates. J Am Chem Soc, 2003, 125(2): 549－553
48 Akiyama Y, Mori T, Katayama Y, Miidome T. The effects of PEG grafting level and injection dose on gold nanorod biodistribution in the tumor-bearing mice. J Control Release, 2009, 139(1): 81－84
49 Didychuk C L, Ephrat P, Chamson-Reig A, Jacques S L, Carson J J L. Depth of photothermal conversion of gold nanorods embedded in a tissue-like phantom. Nanotechnology, 2009, 20(19): 151102－151110
50 Huang Y F, Sefah K, Bamrungsap S, Chang H T, Tan W. Selective photothermal therapy for mixed cancer cells using aptamer-conjugated nanorods. Langmuir, 2008, 24(20): 11860－11865
51 von Maltzahn G, Park J H, Agrawal A, Bandaru N K, Das S K, Sailor M J, Bhatia S N. Computationally guided photothermal tumor therapy using long-circulating gold nanorod antennas. Cancer Res, 2009, 69(9): 3892－3900
52 Goodrich G P, Payne J D, Sharp K, Bao L, Sang K L. Efficacy of photothermal ablation using intravenously delivered NIR-absorbing nanorods in colon cancer. in Energy-based Treatment of Tissue and Assessment, SPIE, 2009
53 Huang X H, El-Sayed I H, Qian W, El-Sayed M A. Cancer cell imaging and photothermal therapy in the near-infrared region by using gold nanorods. J Am Chem Soc, 2006, 128(6): 2115－2120
54 Wang C G, Chen J, Talavage T, Irudayaraj J. Gold nanorod/Fe3O4 nanoparticle "nano-pearl-necklaces" for simultaneous targeting, dual-mode imaging, and photothermal ablation of cancer cells. Angew Chem-Int Edit, 2009, 48(15): 2759－2763
55 Lal S, Clare S E, Halas N J. Nanoshell-enabled photothermal cancer therapy: Impending clinical impact. Accounts Chem Res, 2008, 41(12): 1842－1851
56 Hao E, Li S Y, Bailey R C, Zou S L, Schatz G C, Hupp J T. Optical properties of metal nanoshells. J Phys Chem B, 2004, 108(4): 1224－1229
57 Zhang J Z, Schwartzberg A M, Norman T, Grant C D, Liu J, Bridges F, van Buuren T. Comment on "gold nanoshells improve single nanoparticle molecular sensors". Nano Lett, 2005, 5(4): 809－810
58 Zhang J Z, Wang Z L, Liu J, Chen S, Liu G-y. Self-assembled Nanostructures. Nanoscale Science and Technology. New York: Kluwer Academic/Plenum Publishers, 2003. 316

59 Zhang J Z. Optical Properties and Spectroscopy of Nanomaterials. Singapore: World Scientific Publisher, 2009. 383
60 Schwartz J A, Shetty A M, Price R E, Stafford R J, Wang J C, Uthamanthil R K, Pham K, McNichols R J, Coleman C L, Payne J D. Feasibility study of particle-assisted laser ablation of brain tumors in orthotopic canine model. Cancer Res, 2009, 69(4): 1659－1667
61 Gobin A M, Moon J J and West J L. EphrinA1-targeted nanoshells for photothermal ablation of prostate cancer cells. Int J Nanomed, 2008, 3(3): 351－358
62 Lowery A R, Gobin A M, Day E S, Halas N J, West J L. Immunonanoshells for targeted photothermal ablation of tumor cells. Int J Nanomed, 2006, 1(2): 149－154
63 Bernardi R J, Lowery A R, Thompson P A, Blaney S M, West J L. Immunonanoshells for targeted photothermal ablation in medulloblastoma and glioma: an *in vitro* evaluation using human cell lines. J Neuro-Oncol, 2008, 86(2): 165－172
64 Male K B, Lachance B, Hrapovic S, Sunahara G, Luong J H T. Assessment of cytotoxicity of quantum dots and gold nanoparticles using cell-based impedance spectroscopy. Anal Chem, 2008, 80(14): 5487－5493
65 Hauck T S, Ghazani A A, Chan W C W. Assessing the effect of surface chemistry on gold nanorod uptake, toxicity, and gene expression in mammalian cells. Small, 2008, 4(1): 153－159
66 Parab H J, Chen H M, Lai T C, Huang J H, Chen P H, Liu R S, Hsiao M, Chen C H, Tsai D P, Hwu Y K. Biosensing, cytotoxicity, and cellular uptake studies of surface-modified gold nanorods. J Phys Chem C, 2009, 113(18): 7574－7578
67 Alkilany A M, Nagaria P K, Hexel C R, Shaw T J, Murphy C J, Wyatt M D. Cellular uptake and cytotoxicity of gold nanorods: Molecular origin of cytotoxicity and surface effects. Small, 2009, 5(6): 701－708